

## Search for Violation of Time-Reversal Invariance in Inelastic $e$ - $p$ Scattering\*

J. A. APPEL,<sup>†</sup> J. R. CHEN,<sup>‡</sup> J. SANDERSON, G. GLADDING, M. GOITEIN,<sup>§</sup> K. HANSON, D. C. IMRIE,<sup>||</sup>  
T. KIRK, R. MADARAS, R. V. POUND, L. PRICE, RICHARD WILSON, AND C. ZAJDE\*\*

*Department of Physics, Harvard University, Cambridge, Massachusetts 02138*

(Received 29 September 1969)

Electrons have been scattered inelastically from a hydrocarbon target containing protons polarized normal to the scattering plane. Scattered electrons with energies corresponding to the production of the  $\Delta(1236)$ ,  $N(1512)$ , and  $N(1688)$  pion-nucleon resonances were observed. A search was made for changes in the cross section as the target polarization was reversed. Any changes would have been evidence of a violation of time-reversal invariance in the electromagnetic interactions of the hadrons. No such changes were observed. With the maximum time-reversal-violating effect possible, the asymmetry would be 10 times the upper limit of this experiment. Early attempts at a coincidence-polarization experiment are described in an appendix.

### I. BACKGROUND AND THEORY

#### A. Historical Background

SINCE the discovery of the violation of  $CP$  invariance in the decay of the long-lived neutral  $K$  meson,<sup>1</sup> interest has been revived in the search for violations of time-reversal ( $T$ ) invariance which must occur if the  $CPT$  symmetry is to hold. Previous work had placed a limit of a few percent on possible  $T$ -violating amplitudes in several strong and weak interactions. Furthermore, quantum electrodynamics, which has been so successful in explaining the electromagnetic interactions of photons and leptons, is a  $T$ -invariant theory. Until recently, however, there has been no effective test of  $T$  invariance in the electromagnetic interactions of the strongly interacting particles.

In 1965, Bernstein, Feinberg, and Lee<sup>2</sup> pointed out that just such a violation of  $T$  invariance in the electromagnetic interaction could be responsible for the observed violation of  $CP$  invariance.

If an electromagnetic amplitude is to account for the  $CP$  violation, it would be of comparable size to the usual electromagnetic amplitudes. This fact led Bernstein, Feinberg, and Lee to suggest a new hadronic electromagnetic current  $K_\mu$  which is even under the operation of the time-reversal operator  $T$ . This new current could combine with the usual current  $J_\mu$  (odd under time reversal) to make up the total hadronic electromagnetic current  $\mathcal{J}_\mu$ :

$$\mathcal{J}_\mu = J_\mu + K_\mu. \quad (1)$$

\* Supported by the Atomic Energy Commission.

<sup>†</sup> Present address: Nevis Laboratories, Columbia University, Irvington, N. Y.

<sup>‡</sup> Department of Physics, University of Pennsylvania, Philadelphia, Pa.

<sup>§</sup> University of California, Radiation Laboratory, Berkeley, Calif.

<sup>||</sup> Department of Physics, University College, London, England.

\*\* Laboratoire de l'Accélérateur Linéaire, Orsay, Essonne, France.

<sup>1</sup> J. H. Christenson, J. W. Cronin, V. L. Fitch, and R. Turlay, Phys. Rev. Letters **13**, 138 (1964).

<sup>2</sup> J. Bernstein, G. Feinberg, and T. D. Lee, Phys. Rev. **139B**, 1650 (1965).

In 1966, Christ and Lee<sup>3</sup> refined the idea of the new current  $K_\mu$  and suggested lepton-nucleus scattering tests of  $T$  invariance. The only straightforward experimental test is the scattering of unpolarized leptons from a polarized nucleon target. Elastic lepton-nucleon scattering is not an appropriate reaction for testing  $T$  invariance, since an apparent violation of  $T$  invariance would also be a violation of conservation of the electromagnetic current  $\mathcal{J}_\mu$ , i.e., charge conservation. Thus, Christ and Lee suggested inelastic scattering of leptons from a polarized nucleon target. The work reported here is just such an experiment, the scattering of unpolarized electrons from a target containing polarized protons.

#### B. Theoretical Framework

Using the helicity-amplitude formalism, Christ and Lee<sup>3</sup> defined the three amplitudes (form factors)

$$F_{\pm} = \mp \frac{1}{2} \langle \lambda_{\Gamma} = \frac{1}{2} \pm 1 | \mathcal{J}_x(0) \pm i \mathcal{J}_y(0) | \lambda_N = \frac{1}{2} \rangle, \quad (2)$$

$$F_Z = \langle \lambda_{\Gamma} = \frac{1}{2} | \mathcal{J}_z(0) | \lambda_N = \frac{1}{2} \rangle,$$

where  $\lambda_i$  is the helicity of the state  $i = N$  (nucleon) or  $\Gamma$  (some state excited from the nucleon). Then, assuming Lorentz invariance, parity conservation, conservation of the electromagnetic current, single-photon exchange, quantum electrodynamics for the leptonic part of the interaction, and a vanishing electron mass, one can express the cross section for inelastic electron-

TABLE I. Kinematic regions studied.

| Resonance region | $W_c^a$ (MeV) | $\Delta W$ (MeV) | Electron scattering angle (deg) | Incident electron energy (GeV) | $E_{W'}$ (GeV) | $q_{W'}^2$ (GeV/c) <sup>2</sup> |
|------------------|---------------|------------------|---------------------------------|--------------------------------|----------------|---------------------------------|
| First            | 1229          | 189              | 7.34                            | 3.98                           | 3.52           | 0.23                            |
| Second           | 1529          | 154              | 7.59                            | 5.98                           | 4.98           | 0.52                            |
| Second           | 1507          | 174              | 9.05                            | 5.97                           | 4.85           | 0.72                            |
| Third            | 1690          | 167              | 7.59                            | 5.98                           | 4.66           | 0.49                            |
| Third            | 1686          | 183              | 9.05                            | 5.97                           | 4.56           | 0.68                            |

<sup>a</sup>  $W_c$  is the central value of the pion-nucleon center-of-mass energy in the bin width  $\Delta W$ .  $E_{W'}$  and  $q_{W'}^2$  are the scattered-electron energy and four-momentum transfer for the central energy value  $W_c$ .

<sup>3</sup> N. Christ and T. D. Lee, Phys. Rev. **143B**, 1310 (1966).

nucleon scattering as

$$\frac{d\sigma}{d\Omega_e dE'} = \Gamma_T \{ \sigma_T + \epsilon \sigma_0 + P [2\epsilon(\epsilon+1)]^{1/2} \sigma_{0T} \}, \quad (3)$$

where

$$\begin{aligned} \Gamma_T &= \frac{\alpha K E'}{4\pi^2 q^2 E} \left[ 2 + \frac{\cot^2(\frac{1}{2}\theta)}{1+\tau} \right], \\ \epsilon &= [\cot^2(\frac{1}{2}\theta)] / [2(1+\tau) + \cot^2(\frac{1}{2}\theta)], \\ \tau &= q^2/q_0^2, \\ \sigma_T &= \frac{4\pi^2\alpha}{K} \sum_{\Gamma} [ |F_+|^2 + |F_-|^2 ] \\ &\quad \times \delta(E+M-E'-E'_{\text{hadrons}}), \end{aligned} \quad (4)$$

$$\begin{aligned} \sigma_0 &= \frac{4\pi^2\alpha}{K} \frac{1}{\tau} \sum_{\Gamma} |F_z|^2 \delta(E+M-E'-E'_{\text{hadrons}}), \\ \sigma_{0T} &= \frac{4\pi^2\alpha}{K} \frac{1}{\sqrt{\tau}} \sum_{\Gamma} \eta \text{Im} F_-^* F_z \delta(E+M-E'-E'_{\text{hadrons}}), \end{aligned}$$

with

$$\eta = \pi_N \pi_{\Gamma}^{-1} e^{i\pi(J_N - J)},$$

and where  $J_N = \frac{1}{2}$  is the spin of the nucleon,  $J_{\Gamma}$  is the spin or total angular momentum of the state  $\Gamma$ ,  $\pi_N$  is the parity of the nucleon,  $\pi_{\Gamma}$  is the parity of the state  $\Gamma$ , and  $P$  is the polarization of the initial nucleon normal to the scattering plane. The notation differs slightly from that in Ref. 3 but conforms to the usage common in electron scattering experiments.

The statement of  $T$  invariance is that  $\sigma_{0T} = 0$ , since then  $F_-$  and  $F_z$  are relatively real. The relative reality of the  $F$ 's requires that the current operators  $\mathcal{J}_{\mu}$  be evaluated between particular helicity states  $|\lambda_i\rangle$ . In particular, the states must be eigenstates of the strong-interaction Hamiltonian  $H_{st}$  and an operator  $T_{st} e^{-i\pi J_y}$ , i.e.,

$$O|\lambda_i\rangle = T_{st} e^{-i\pi J_y} |\lambda_i\rangle = \eta_i^* \langle \lambda_i |, \quad (5)$$

where  $J_y$  is the  $y$  component of the total angular momentum operator and  $\eta_i$  is a phase factor independent of the helicity of the state  $i$ . Then,

$$F_{\pm}/F_{\pm}^* = \eta_{\Gamma} \eta_N^* = F_z/F_z^*. \quad (6)$$

The requirement that the form factors  $F$  be evaluated with eigenstates of the strong Hamiltonian corresponds to the experimental requirement of detecting incident and final hadron states which are also eigenstates of the strong Hamiltonian. The initial polarized proton, which is the nucleus of a hydrogen atom in the target, is, of course, an eigenstate of  $H_{st}$ . If, on the other hand, a particular charge mode of the excited state were detected, say,  $p + \pi^0$ , then the final state would *not* be an eigenstate of  $H_{st}$ . The summation of all contributions

to a resonance at a given energy or of all the continuum states at a given energy would form eigenstates of  $H_{st}$ . Similarly, if one could isolate all contributions to a given total angular momentum or a given isospin at some energy, then one would have an eigenstate of  $H_{st}$ .

The problem of isolating the contributions of a particular resonance or a particular total angular momentum state would require great experimental and analytic capability. However, if one agrees to sum over all outgoing hadron states with a given energy [the sums over  $\Gamma$  in Eq. (4)], then one will have an eigenstate of  $H_{st}$  without the complications just described. Thus, the experimental test of time reversal discussed here was a single-arm measurement. Only the scattered electrons of a given energy  $E'$ , corresponding to a given energy of the hadron state  $\Gamma$ , were detected.

### C. Theoretical Asymmetry and "Maximal Effect"

Given the cross section in Eq. (3), one can define an asymmetry  $\alpha$  for protons whose spin is perpendicular to the scattering plane:

$$\alpha = (\sigma_+ - \sigma_-) / (\sigma_+ + \sigma_-), \quad (7)$$

where  $\sigma_+$  ( $\sigma_-$ ) represents the doubly-differential cross section  $d\sigma/dE'd\Omega_e$  with the spin of the target nucleon parallel (antiparallel) to the normal to the scattering plane,  $n$ . Then

$$\alpha = \sqrt{2}\epsilon(\epsilon+1)\sigma_{0T}/(\sigma_T + \sigma_0\epsilon), \quad (8)$$

$$\alpha = \sqrt{2}\epsilon(\epsilon+1) \frac{\sum_{\Gamma} (\eta/\sqrt{\tau}) |F_-| |F_z| \sin\delta_{\Gamma}}{\sum_{\Gamma} [ |F_+|^2 + |F_-|^2 + (\epsilon/\tau) |F_z|^2 ]}, \quad (9)$$

where the sum is understood to apply only to states which conserve energy and  $\delta_{\Gamma}$  is the relative phase between  $F_{\pm}$  and  $F_z$  for the state  $\Gamma$ .

#### 1. "Maximal-Effect" Model

In order to obtain an estimate of a "maximal effect," we make the following assumptions:

(a) All terms in the sum over  $\Gamma$  have the *same* phase  $\delta$  and one term dominates.

(b) The hadronic helicity amplitudes  $F_-$  and  $F_+$  are related by a *constant*  $A$ , i.e.,

$$A = \eta |F_-| / [ \sum_{\Gamma} ( |F_+|^2 + |F_-|^2 ) ]^{1/2}. \quad (10)$$

The asymmetry can then be expressed as

$$\alpha = [2\epsilon(\epsilon+1)]^{1/2} A \left( \frac{R}{1+\epsilon R^2} \right) \sin\delta, \quad (11)$$

where  $R$  is the ratio of scalar to transverse amplitudes, i.e.,

$$R^2 = \frac{\sigma_0}{\sigma_T} = \frac{\sum_{\Gamma} (1/\tau) |F_z|^2}{\sum_{\Gamma} ( |F_+|^2 + |F_-|^2 )}. \quad (12)$$

For forward-angle scattering,  $\epsilon$  is very near to 1. For the angles in this experiment,  $\epsilon \geq 0.95$ , and we can consider

$$\alpha \sim 2A \left( \frac{R}{1+R^2} \right) \sin \delta. \quad (13)$$

As can be seen from the symmetry of this expression in terms of  $R$  and  $1/R$ , there is little sensitivity to  $R$  for  $R$  near 1. This is a fortunate property because the values of  $R$  are not well known throughout the region of interest. Furthermore, for  $R$ ,  $A$ , and  $\sin \delta \sim 1$ , the asymmetry is also  $\sim 1$ , corresponding to a large experimental effect. The experiment described herein was designed to search for just such a possibility.

### 2. Other Models for $T$ -Violation Effect

There is interest in possible  $T$ -violation effects for more restricted models than those in the class just discussed. For example, the time-reversal violation may be restricted to (1) resonant single-pion production or (2) an interference between the resonant and background amplitudes. In these cases,  $\sigma_{\theta T}$  contains only those amplitudes which interfere to give a  $T$ -violation effect. The resultant predicted asymmetry  $\alpha$  is, therefore, smaller than it was for the class of models discussed in the previous section.

One can still use Eq. (11) to estimate the  $T$ -violating phase angle  $\delta$ . However, one must make the substitution

$$A \rightarrow A' = A f_1 f_2, \quad (14)$$

where

$$f_1 = \frac{(F_-)_{\text{restr}}}{(F_-)_{\text{tot}}} \quad \text{and} \quad f_2 = \frac{(F_z)_{\text{restr}}}{(F_z)_{\text{tot}}}.$$

In these models, we again make the assumptions of the appropriateness of a single phase angle  $\delta$  and a constant  $A'$ .

### D. Problems of Interpretation

Had a large asymmetry been found, it would have been difficult to interpret except as an evident violation of time-reversal invariance in the electromagnetic interaction. No such large asymmetry was found. The interpretation of a small asymmetry is impeded by two effects: (1) possible non- $T$ -violation effects due to two-photon exchange and (2) lack of a compelling model for time-reversal noninvariance itself.

#### 1. Two-Photon-Exchange Effects

In the derivation of the asymmetry formulas, the single-photon-exchange approximation was made. Effects due to a two-photon amplitude might first appear as an interference with the larger single-photon-exchange amplitude. Such an interference would be suppressed by an additional factor of  $\alpha = 1/137$ . This implies that two-photon-exchange effects are totally

negligible at the level of accuracy obtained in this experiment. No evidence of unexpected enhancements in other two-photon-exchange experiments has been observed.<sup>4-8</sup>

#### 2. Lack of Compelling Model

A more serious problem of interpretation arises from the lack of a specific model to be tested. The addition of the current  $K_\mu$  is a framework within which it may be convenient to define a model. Lee has suggested two such models,<sup>9</sup> but has not calculated the expected effect of either on inelastic lepton scattering.

In essence, we must think of the time-reversal experiment as a *search* for  $T$  violations in the electromagnetic interaction more than as a *test* of  $T$  invariance in electromagnetic interactions. The same is true, of course, for all the so-called tests of invariances which produce null results.

### E. Selection of Kinematic Regions for Study

It is evident from the preceding theoretical framework that an effect due to time-reversal violation may manifest itself in an interference between scalar and transverse production amplitudes. It is necessary, then, to select kinematic regions in which both scalar and transverse production amplitudes exist and are of comparable magnitude.

There is direct experimental evidence that there are large scalar production amplitudes in the first resonance region for momentum transfers of 3 and 6  $F^{-2}$  [0.12 and 0.24  $(\text{GeV}/c)^2$ ].<sup>10-12</sup> The resonance itself is dominantly transversely produced, as is well known.<sup>10</sup> It is possible to imagine, therefore, a time-reversal noninvariance manifested through an interference between the resonant and background amplitudes. Such an effect would be largest between the threshold and peak of the resonance, since it is in these regions that the scalar and transverse amplitudes, respectively, are largest. A search for structure in the asymmetry as a function of excitation energy  $E'$  can be made to look for such behavior.

Similarly, both longitudinal and transverse contributions are known to exist in the production of the higher

<sup>4</sup> J. Mar, B. C. Barish, J. Pine, D. H. Coward, H. DeStaebler, J. Litt, A. Minten, R. E. Taylor, and M. Breidenbach, *Phys. Rev. Letters* **21**, 482 (1968).

<sup>5</sup> F. Guerin and C. A. Pikketty, *Nuovo Cimento* **32**, 971 (1964).

<sup>6</sup> J. C. Bizot, J. M. Buon, J. Lefrançois, J. Perez-y-Jorba, and P. Roy, *Phys. Rev.* **140**, B1387 (1965).

<sup>7</sup> G. V. DiGiorgio, E. Ganssauge, R. Gomez, G. Gorini, S. Penner, S. Serbassi, M. L. Vincelli, E. Amaldi, and G. Stoppini, *Nuovo Cimento* **39**, 474 (1965), and references therein.

<sup>8</sup> G. K. Greenhut, thesis, Cornell University, 1968 (unpublished).

<sup>9</sup> T. D. Lee, *Phys. Rev.* **140**, B959 (1965); **140**, B967 (1967).

<sup>10</sup> H. L. Lynch, J. V. Allaby, and D. M. Ritson, *Phys. Rev.* **164**, 1635 (1967).

<sup>11</sup> J. Peres-y-Jorba and D. Treille, *Nucl. Phys.* **B5**, 355 (1968).

<sup>12</sup> C. Mistretta, D. Imrie, J. A. Appel, R. Budnitz, L. Carroll, J. Chen, J. Dunning, M. Goitein, K. Hanson, A. Litke, and R. Wilson, *Phys. Rev. Letters* **20**, 1070 (1968).

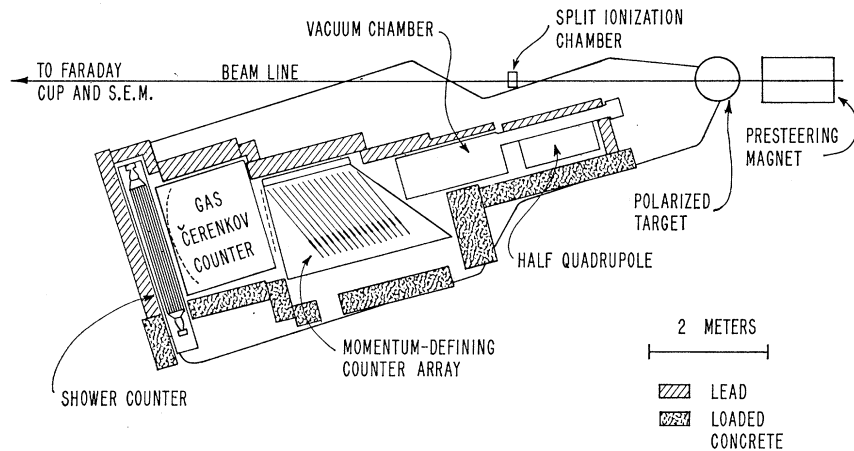


Fig. 1. Plan view of the apparatus.

resonances.<sup>13</sup> However, the analysis of these deeper inelastic regions is not as complete as it is for the first resonance region.

The kinematic regions studied were chosen with the aim of maximizing the possible asymmetry for a given  $\sigma_0$ ,  $\sigma_T$ , and  $q^2$ . From Eq. (3) we see that this is always obtained at the highest possible energy. The regions are listed in Table I.

## II. EXPERIMENTAL CONSIDERATIONS

In this experiment, we measure the doubly-differential cross section  $d\sigma/d\Omega_e dE'$  [Eq. (3)] for inelastic electron scattering from polarized protons with both signs of polarization. Thus, the electrons scattered into our angular acceptance are detected and momentum-analyzed (Figs. 1 and 2). The numbers of electrons accepted are then used to compute the asymmetry due to any changes in cross section correlated with the proton polarization.

Since this is an asymmetry measurement, stability is the all-important feature in the experiment. Furthermore, not very great precision is required of the absolute numbers which are to be determined. For example, the solid angle, energy bite, and detection efficiencies need not be determined if they do not change. Since both cross sections in the asymmetry are measured with the same spectrometer and without changes in magnetic fields or typical scattering trajectories, the above factors tend to cancel out of the asymmetry.

### A. Apparatus and Experimental Procedure

An external electron beam of the Cambridge electron accelerator was directed at a target containing polarized protons. The unscattered beam was directed through position-monitoring split ionization chambers into a Faraday cup. Charged particles scattered at forward angles to the incident electron beam were momentum-

analyzed in a spectrometer consisting of a half-quadrupole magnet and 25 scintillation counters. Separation of electrons from other charged scattering products was accomplished with the combined use of a threshold gas Čerenkov counter and lead-Lucite shower counter. Only the scattered electrons were detected in this experiment.

Data were stored, event by event, on magnetic tape using a PDP-1 on-line computer, which permitted experimental checks during data acquisition and detailed postrun analysis.

The electron detection apparatus used in this experiment was also used in three previous experiments.<sup>13-15</sup> In fact, the consistency on the 1% level of measurements of elastic cross sections made six months apart gives confidence in the basic stability of the apparatus. Since the electron detection apparatus has been described in papers associated with these earlier experiments, only the new features of the apparatus will be discussed: the polarized proton target, the new characteristics of the incident electron beam, and the split ionization chamber used as a beam-position monitor.

#### 1. Target

The major new feature of the apparatus for this experiment was the polarized target built by Sanderson, Chen, and Pound. The target and its operation are described elsewhere.<sup>16</sup> Only a very brief description will be given here.

The target material was a mixture of ethanol and water doped with a paramagnetic material, porphyraxide. The target was cooled to about 1°K with pumped liquid helium. A pair of superconducting Helmholtz coils produced a uniform 25-kG magnetic field at the

<sup>14</sup> R. J. Budnitz, J. Appel, L. Carroll, J. Chen, J. R. Dunning, Jr., M. Goitein, K. Hanson, D. Imrie, C. Mistretta, J. K. Walker, and R. Wilson, *Phys. Rev.* **173**, 1357 (1968).

<sup>15</sup> M. Goitein, R. J. Budnitz, L. Carroll, J. Chen, J. R. Dunning, Jr., K. Hanson, D. Imrie, C. Mistretta, J. K. Walker, R. Wilson, G. F. Dell, M. Fotino, I. M. Paterson, and H. Winick, *Phys. Rev. Letters* **18**, 1016 (1967).

<sup>16</sup> J. Sanderson, J. R. Chen, and R. V. Pound (unpublished).

<sup>13</sup> A. A. Cone, K. W. Chen, J. R. Dunning, Jr., G. Hartwig, N. F. Ramsey, J. K. Walker, and R. Wilson, *Phys. Rev.* **156**, 1490 (1967).

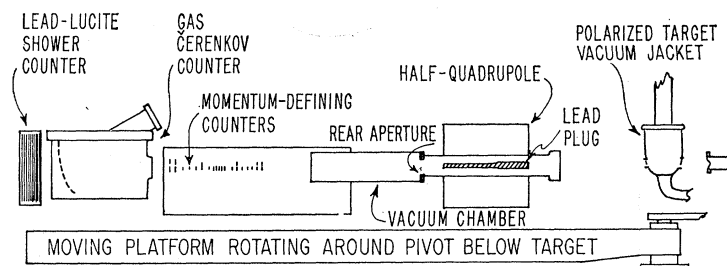


Fig. 2. Side view of the apparatus.

center of the target. At these low temperatures and high magnetic field, the paramagnetic impurity is highly polarized ( $\sim 88\%$ ). The free protons in the target are not significantly polarized, since the proton magnetic moment is approximately  $1/1000$  that of the paramagnetic center. However, simultaneous spin flips of the free protons (those not bound to other nucleons) and the paramagnetic centers can be induced by applying a suitable rf signal.<sup>17</sup> Since the relaxation time of the free-proton polarization is long compared to the relaxation time of the paramagnetic centers, it is possible to polarize many protons with a single paramagnetic center. Spin exchange among the free protons helps to propagate the polarization from a single paramagnetic center beyond the region of direct interaction. Free-proton polarization was typically  $22\%$  at the beginning of a data run. The polarizable protons are the nuclei of the hydrogen atoms in the target. The protons in the heavier nuclei are unpolarized, since pairing in the heavier nuclei results in zero net spin. The sample contained about  $92\%$   $C_2H_5OH$  and  $8\%$   $H_2O$ , so that  $23\%$  of the protons or  $13\%$  of the nucleons were polarizable. The measured target polarization must be reduced by this factor in calculating the asymmetry of the scattering from a single proton.

Because of the radiation damage to the target, it was necessary to change frequently the section of target being irradiated. At the same time, it was necessary to maintain the target density for a pair of cross-section measurements for each asymmetry determination. Thus, after every pair of runs, the target material was raised or lowered by remote control. This motion required only a few seconds and caused no change in the scattering geometry.

All the beam always passed through the target, and the target had a constant thickness of approximately  $2.5$  cm. The target was moved  $0.3$  mm each time and the beam was focused to  $1$  mm at the target. The targets were generally operated until the polarization was reduced to  $60\%$  of the original polarization.

The net target polarization was determined from the free-proton polarization, which was measured using the

proton nuclear-magnetic-resonance signal. The absolute free-proton polarization was determined by normalizing the polarized proton signal to the thermal-equilibrium proton signal.

The nuclear magnetic resonance monitored the average free-proton polarization over the entire sample. Thus, a geometrical correction always had to be applied in order to determine the fraction of target already irradiated. The average polarization in the irradiated section was calculated from the initial and final polarizations thus obtained. The polarization monitor had a long time constant compared to an electron-beam pulse and could not be used to monitor the instantaneous value of the polarization during a single beam pulse, even of the total sample.

The difference in polarization for the spin-up and spin-down cross-section measurements enters the asymmetry as a normalization factor and had to be measured.

## 2. Thermal Depolarization

The radiation damage to the target resulted in a permanent reduction in the polarization. In addition, there can be reversible changes due, for example, to temperature changes in the target. The target is cooled by superfluid helium and the sample is powdered to prevent appreciable temperature gradients across the target material.

In order to check this, a special run was made when the whole target was irradiated with a beam of three times the current density used in the data runs. The data runs used a beam of  $3 \times 10^{-9}$  A. The average polarization of the whole target was observed. After  $\frac{1}{2}$  min a pressure rise in the helium occurred as the vacuum pumps failed to cope with the increased evaporation; the polarization varied in a manner consistent with the temperature of the target but nothing was found to indicate any loss of polarization due to direct effects of the electron beam.

The nuclear-magnetic-resonance measurement still averaged over a time long compared to a beam pulse (about  $100 \mu\text{sec}$  beam on and  $16$  msec beam off). Since the time required to polarize the sample to  $90\%$  of its maximum polarization is several seconds, it is difficult to conceive any mechanism that would let the polarization change from its average value during the  $16$  msec interval between pulses.

<sup>17</sup> M. Borghini, in *Proceedings of the International Conference on Polarized Targets and Ion Sources, Saclay, France, 1966*, edited by La Direction de la Physique, Centre d'Etudes Nucléaires de Saclay (Centre d'Etudes Nucléaires de Saclay, Gif-sur-Yvette, France, 1967).

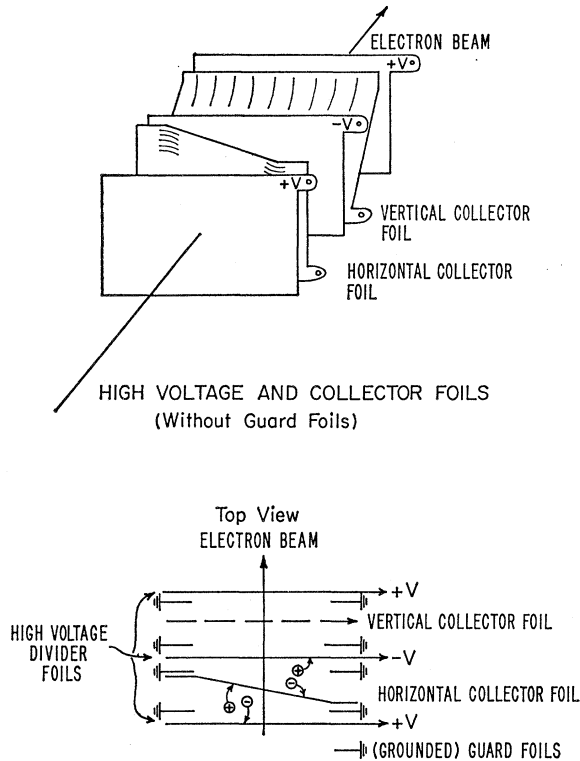


FIG. 3. Schematic views of the split ionization chamber. Top: high voltage and collector foils (without guard foils); bottom: top view.

### 3. New Characteristics of Beam

In order to correct for the effect of the target magnetic field, a presteering magnet was placed upstream of the target. The electron beam was thus directed into the Faraday cup and the target itself was positioned in the deflected beam line. The new target location affected the magnitude of the electron solid angle (1.4 msr at 4 GeV and 1.7 msr at 6 GeV) and the calibration of the spectrometer (0.1%). However, no loss of stability resulted from these changes.

The quadrupole magnets in the beam-transport system allowed a choice of focusing properties for the extracted beam. When the beam was first set up, it was focused horizontally at the split ionization chamber and vertically just downstream of the target.

This choice of horizontal focusing was aimed at (1) keeping the current density low at the target in order to reduce depolarization effects and (2) minimizing the variations in scattering angle due to horizontal spread in the beam and fluctuations in the beam position at the target.

The choice of vertical focusing was designed to aid the resolution of the spectrometer system. The vertical extent of the beam contributed about 3.5% full width at half-maximum (FWHM) to the momentum resolution.

### 4. Split Ionization Chamber

This experiment is the first to make use of a split ionization chamber in an intense beam of high-energy electrons. For this reason, and since the chamber served as a monitor of changes in the scattering angle, it is described in some detail below.

The split ionization chamber is shown schematically in Fig. 3. The electron beam ionizes molecules of gas along its path in the ionization chamber. The number of ions produced is directly proportional to the path length of the electron beam in the gas. The chamber is divided into two independent sections, one each for determining the horizontal and vertical positions of the beam at the chamber. A collector foil separates each section into two parts. The collector foils gather positive charge from one side of the chamber and negative charge from the other. The collector foils are sloped so that the position of the beam determines the ratio of positive to negative charge collected. There is one position of the beam at which the amounts of positive and negative charge will just equalize. This is the nominal center of the chamber. For the horizontal coordinate, it was possible to locate this nominal center by moving the chamber relative to the beam. The position of the chamber was determined with the use of a linear potential divider fixed with respect to the flux-return piece of the half-quadrupole magnet. The chamber was calibrated by moving it with respect to the beam in the horizontal direction (Fig. 4). The vertical position was not movable and the chamber output had a constant offset. The sensitivity of the vertical system was calculated from the measured horizontal sensitivity.

The chamber was filled with a mixture of 90% He and 10% N<sub>2</sub> at slightly above atmospheric pressure. The windows of the chamber were made of 1½-mil sheets of stainless steel and the foils in the chamber were 1-mil sheets of aluminum. The measured sensitivity was 19 ion pairs/cm/incident electron, indicating a recombination and collection inefficiency of about 20%.

The output of the chamber was integrated and the integral was taken as a measure of the time-averaged beam position at the chamber.

### 5. Data Acquisition

The method of data acquisition was designed to minimize the need for run-to-run corrections.

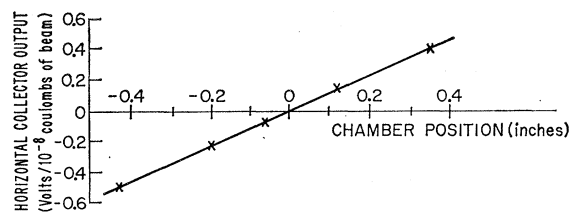


FIG. 4. Sensitivity curve of horizontal split ionization chamber (beam intensity  $2 \times 10^{-9}$  A).

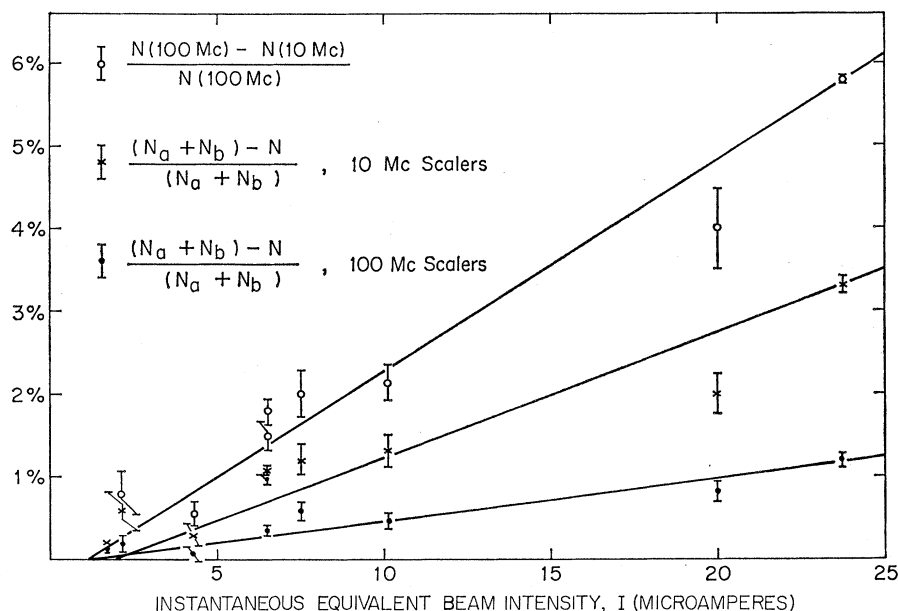


FIG. 5. Intensity dependence of potential computer trigger rate (data taken with  $I < 5$  nA by varying the duty cycle).

The paired data runs were of short duration, typically 3 min. Time between runs was kept at a minimum, typically  $\frac{1}{2}$  min. The point of this brevity was to minimize the time available for unknown systematic drifts in apparatus behavior.

The ordering of runs was designed to cancel first- and second-order systematic drifts. For most of the data, the ordering is as shown in Fig. 15(a), where vertical slashes represent motion of the target in order to expose a new section to the beam. The symbol  $\uparrow$  ( $\downarrow$ ) represents a cross-section measurement with the spin parallel (antiparallel) to the normal of the scattering plane,  $n$ . An asymmetry was determined from each pair of runs between target motions. Only for the first part of the data taken with a scattering angle  $\theta = 7.59^\circ$  did we use the less advantageous ordering represented by Fig. 15(b). This ordering fails to cancel second-order drifts.

No intentional changes in the apparatus other than the change in polarization were ever made except when the target was also being moved. Changes in polarization were accomplished by changing one microwave frequency in the target by 0.3%, which had no effect on the electron beam. If a machine control was noted to have drifted or if there were some other reason to change a part of the apparatus, the change was made only after a series of four or eight runs was completed. Never was a change made between two runs which were to be used together for an asymmetry measurement.

### B. Explicit Parameters

The explicit parameters which enter an asymmetry measurement include the total incident charge, solid angle, momentum bite, number of target particles, and detection efficiency. Of these, only the incident

charge is measured for each cross-section determination (run). The basic stability of the apparatus leads to the cancellation of the other parameters and no run to run corrections were applied for instabilities in these parameters.

The stability of the Faraday cup [efficiency of  $(100 \pm 0.4)\%$ ] is thought to be at least as good as 0.1% over the period of a pair of runs. This stability can be inferred from the stability of the ratio of the incident charge as measured by the Faraday cup and by a secondary-emission monitor. Previous tests<sup>18</sup> with negligible material in the electron beam gave a ratio stable to 0.2% over 10-min periods. In this experiment, the ratio was stable to about  $\frac{1}{2}\%$  but the difference is attributed solely to the secondary-emission monitor, which is thought to be much more sensitive to beam spray, halo, and material in the beam line.

The basic stability of the parameters which cancel in the asymmetry determination is due to the fact that both cross-section measurements are made in close time proximity with no changes in the location of the apparatus, magnetic fields, typical scattering trajectories, or counter system. Motion of the target material to irradiate new material was allowed only after a pair of cross-section determinations. Of the canceling parameters, only the efficiency varies detectably. In selecting various biases in the data analysis, those which appeared to be most stable were used with the exception of the Čerenkov- and shower-counter biases as discussed below.

#### 1. Momentum Counters and Triggering Efficiency

The first element in defining an event trigger was coincident counts in the momentum-defining counters,

<sup>18</sup> F. Dell and M. Fotino, Cambridge Electron Accelerator Report No. CEAL-1043 (unpublished).

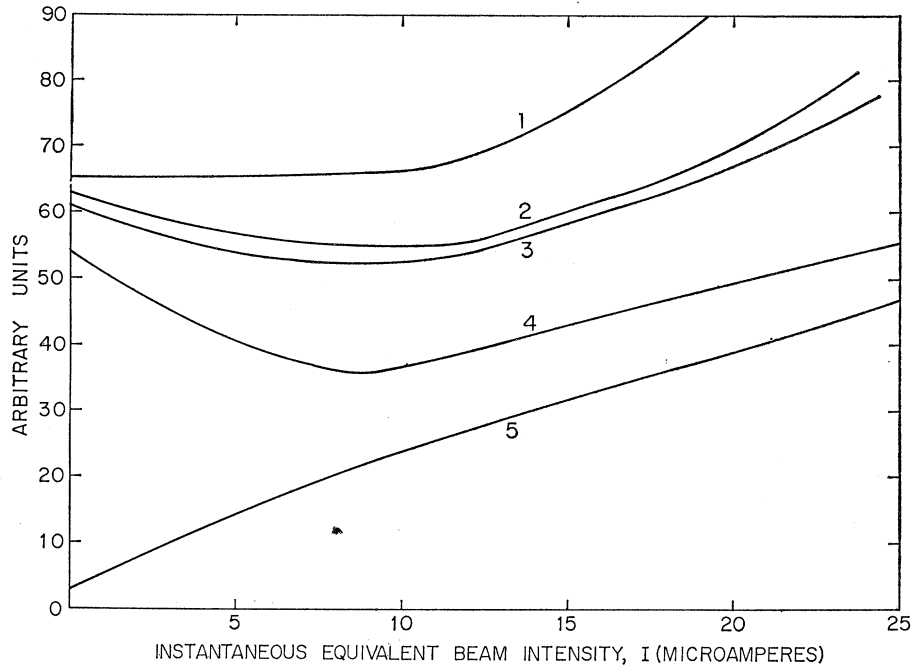


FIG. 6. Intensity dependence of computer-analyzed cross sections (data taken as for Fig. 5). Curve 1, up to two erroneous counter signals; 2, up to one excess or one missing counter signal; 3, up to one apparent excess counter signal; 4, apparently perfect momentum-definition patterns; 5, non-analyzable patterns.

indicating that a charged particle might have crossed the focal plane of the magnet within the acceptable momentum region. If the signals from the Čerenkov and shower counters were above certain minimum levels and if certain nonrestrictive logic conditions were met, an event trigger was formed which resulted in the condition of each counter and relevant analog information being fed to an on-line computer. An analysis of the pattern of counters on and off in the defining array determined whether an event was acceptable, and if so, what momentum would be assigned to it. Thus, variations in efficiency enter at two levels, efficiency of triggering and interpretability of the recorded data.

The trigger rate was monitored separately on 100- and 10-Mc/sec scalars. A slight difference was due to the dead time and became a check of duty cycle or intensity fluctuations (Fig. 5). We also monitored on separate scalars the rates for events with the electron scattered

above or below the central plug of the quadrupole magnet,  $N_a$  or  $N_b$ , as well as the coincident rate  $N=N_a$  and  $N_b$ .

The randoms rates in the momentum-definition counters were particularly sensitive to beam intensity as implied by Fig. 6. However, the trigger requirements were such that there appears no inefficiency in the trigger rate and the effect of an overefficiency is merely to smear out the momentum resolution slightly.

Typical intensity variations within a pulse were on the order of 40%, while pulse-to-pulse intensity variations were about 15%. The average intensity over the period of a pair of runs, however, was usually stable to 10%.

The stability of the counting rate in the face of typical intensity fluctuation encountered in the experiment was better than 0.2% between a pair of runs. No correction, therefore, was applied for this effect.

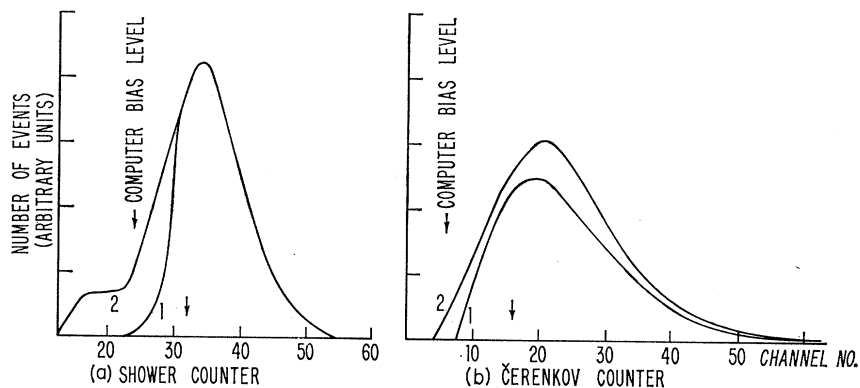
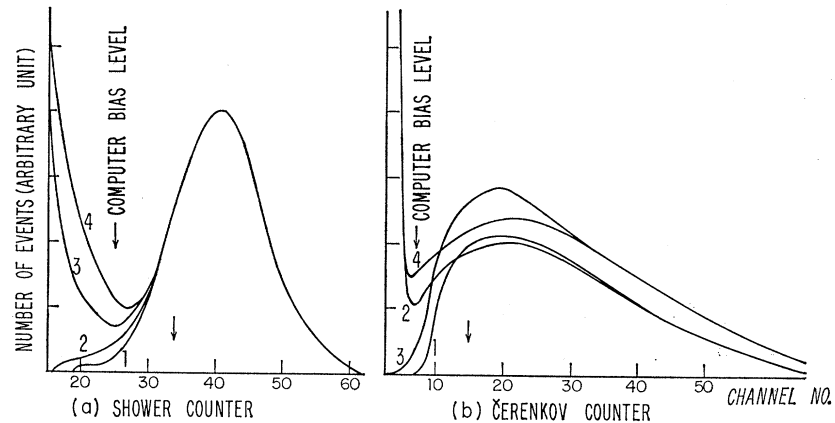


FIG. 7. Shower and Čerenkov counters. Typical spectra for low-energy runs,  $\theta=7.34^\circ$ . Curve 1, trigger configuration for data acquisition; 2, 6 dB removed from before shower-counter discriminator. High bias level used in the analysis (see text) indicated by unlabeled arrows.

FIG. 8. Shower- and Čerenkov-counter typical spectra for high-energy runs. Curve 1, both shower and Čerenkov counters required in trigger (configuration for data acquisition at  $\bar{\theta}=9.05^\circ$ ); 2, only the shower-counter requirement in trigger (configuration for data acquisition at  $\bar{\theta}=7.59^\circ$ ); 3, reduced (6 dB) shower-counter requirement in trigger; 4, reduced (6 dB) shower- and no Čerenkov-counter requirements in trigger. High bias level analyses used levels indicated by unlabeled arrows.



## 2. Čerenkov and Shower Counters

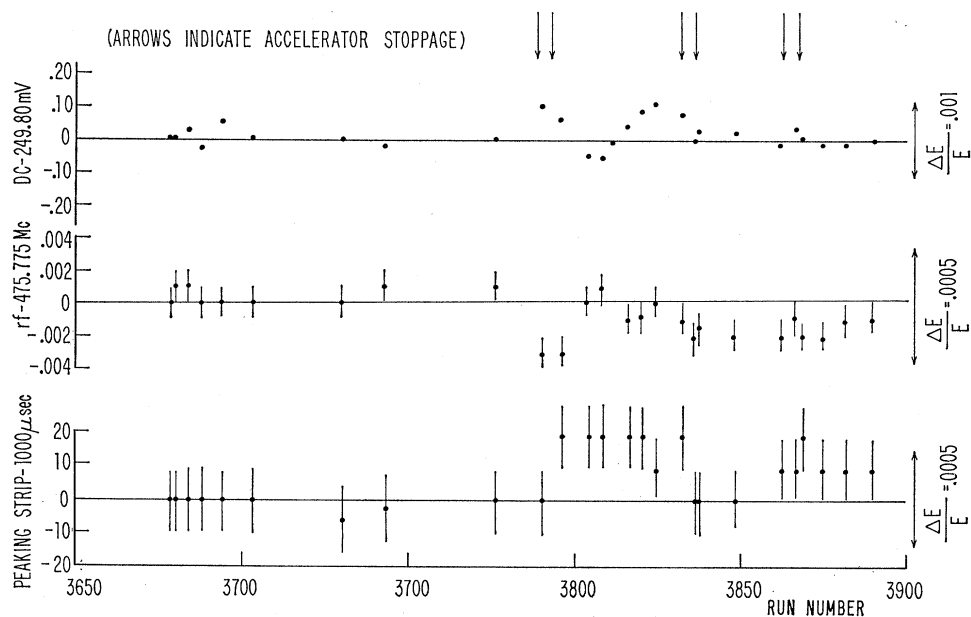
The possibility of random double coincidences causing a trigger was greatly reduced by the Čerenkov- and shower-counter requirements in the trigger. These counters were used to identify the electrons which crossed the magnet focal plane. Figures 7 and 8 show the pulse-height spectra in each of these counters along with the triggering pulse height and the pulse height required of events in the final analyses. Coincident large pulses in each of these counters serve as a firm identification of an electron. In order to check for charged-pion contamination, asymmetry analyses were carried out for several different Čerenkov- and shower-counter biases.

From the spectrum of pulse heights in the shower counter, it is easy to see that slight shifts in gain would have a significant effect on the triggering efficiency, especially for the runs at the first resonance (Fig. 7).

The stability of the peak location and, therefore, of the gain of the shower-counter system was about 0.5 channel over the course of 1 h. At the first resonance, where particular attention was focused on avoiding useless computer triggers, the shower-counter discriminator cut significantly into the otherwise acceptable spectrum. Over a pair of data runs, the triggering efficiency was only stable to 0.6%/run pair (see Fig. 7). This is the largest instability at the first resonance for which no corrections were made. However, the ordering of data acquisition averages the effects of these efficiency drifts.

In the higher-resonance-region runs, the discriminator cut much less severely into the spectrum of otherwise acceptable events. The stability was correspondingly better, i.e., 0.13% per pair of runs. The additional uncertainty due to instability of the computer bias level is insignificant, since the computer discrimination level is applied to such a small fraction of the remaining events.

FIG. 9. Long-term drifts in machine parameters,  $E=4$  GeV/c,  $\bar{\theta}=7.34^\circ$ .



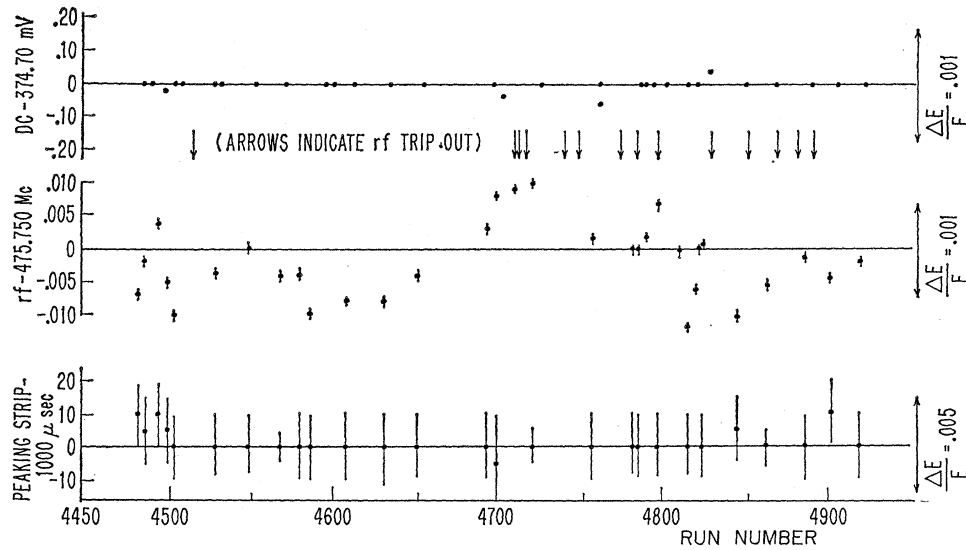


FIG. 10. Long-term drifts in machine parameters,  $E=6$  GeV/c,  $\bar{\theta}=9.05^\circ$ .

At the high scattered energies detected in this experiment (3.3–5.1 GeV), the threshold gas Čerenkov counter could not be operated at near 100% efficiency for electrons and still reject pions. The electron inefficiency of the Čerenkov counter at the highest energies is clear from Fig. 8(b). Nevertheless, the Čerenkov counter was used in the trigger for nearly all of the data except at  $\theta=7.59^\circ$ .

The same stability problem exists for the Čerenkov counter as for the shower counter. For the runs in the region of the first resonance, the Čerenkov-counter efficiency was high. The slight shifts in gain are negligible, since the discriminator cutoff operates on such a small fraction of the events. Thus, the use of the Čerenkov counter in the trigger served to ensure the acceptance of only electrons without adding significant uncertainties due to trigger instability. At the highest-energy runs, the problem of Čerenkov-counter instability enters at the trigger level ( $\theta=9.05^\circ$ ) or at the computer reanalysis level ( $\theta=7.59^\circ$ ). Even ignoring the statistical fluctuations caused by the true electron pedestal events and the random-rate probability of pedestal events appearing in the accepted sample, it is difficult to estimate the size of the potential instability.

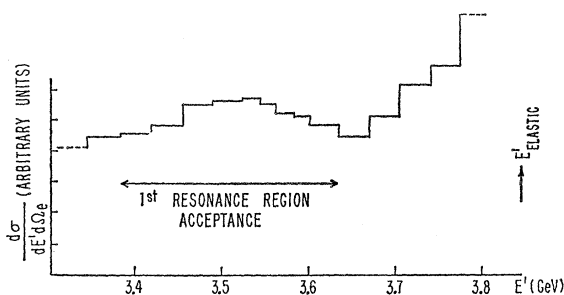


FIG. 11. Scattered-electron spectrum,  $E=4$  GeV/c,  $\bar{\theta}=7.34^\circ$ . Data with regular trigger. Relative bin-size uncertainty = 5%.

However, we believe that any instabilities are less than 1% over the course of a pair of runs and, as was the case for the shower-counter instability in the lower-energy runs, trust to the ordering of data acquisition to average out the effects of these efficiency drifts.

### C. Implicit Parameters

Owing to the greater sensitivity of the asymmetry to drifts in the implicit parameters, great care was taken to monitor these parameters during the data acquisition. As is clear from the monitors of the incident and scattered electron energies and scattering angle, the stability of the implicit parameters was easily sufficient when compared to the final statistical uncertainty obtained in the experiment ( $\sim 10^6$  events per resonance region).

The incident electron energy was determined by three parameters which indicated the performance of the accelerator. Run-to-run corrections due to changes in the average magnetic field during external beam spill were applied to the data. This correction covers variations in the two parameters labeled DC and Peaking Strip in Figs. 9 and 10. Even in the 4-GeV data runs, where the variations are largest, the instabilities are less than 0.02% in energy or less than 0.1% in cross section per pair of runs. No-run to run corrections were made for instabilities in the third parameter, the frequency of the rf signal applied to the accelerating cavities. However, even in the worst case (Fig. 10) the instabilities were less than 0.2% in cross section for a pair of measurements.

The scattered-electron energy was determined by the magnetic field in the half-quadrupole magnet and the counter locations with respect to the magnetic field. The field strength was stable to better than 0.1% per pair of runs and the apparatus locations were static during the course of a series of runs. Furthermore, the

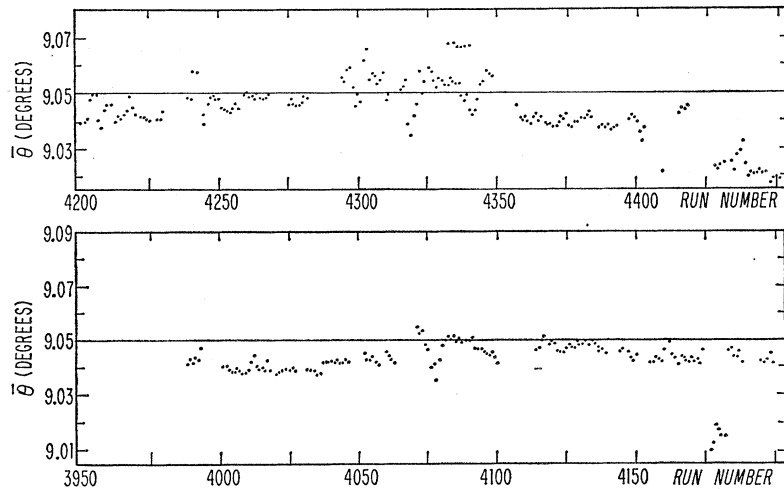


FIG. 12. Drifts in electron scattering angle  $\bar{\theta}$ ,  $E=6$  GeV/c,  $\bar{\theta}=9.05^\circ$ .

spectrum of scattered particles was fairly flat (see, for example, Fig. 11), so that the effect of slight shifts in the analyzing magnetic field would only shift the spectrum slightly, causing only negligible minor changes in counting rate.

The electron scattering angle was monitored by the split ionization chamber. Typical variations in the scattering angle (Fig. 12), caused by shifts in the incident beam direction, were less than  $0.01^\circ$  between pairs of runs used for an asymmetry determination. The consequent changes in the measured cross section were less than  $0.1\%$  per run pair.

Thus, the instability in the individual asymmetry measurements before making any corrections for drifts in the implicit parameters was no larger than the statistical uncertainty of the final averaged asymmetry. Since we corrected for most of the induced instability by the implicit parameters run by run, and since the final asymmetry was the average of many such asymmetry measurements, the effects of drifts in the implicit parameters was negligible (and, in fact, the corrections did not change the results).

#### D. Normalization

The physically meaningful asymmetry  $\alpha$  is given in terms of the cross sections for 100%-polarized free protons by

$$\alpha = (\sigma_+ - \sigma_-) / (\sigma_+ + \sigma_-).$$

The measured cross sections  $\Sigma_{\pm}$  are not equal to  $\sigma_{\pm}$  for two reasons: (1) The free protons in the target are not 100% polarized, but have an effective polarization  $P$ , the average of the magnitudes of the "up" and "down" polarizations, and (2) there is contaminating material in the target consisting of unpolarized bound nucleons (both protons and neutrons) in (a) the target material itself and (b) the target walls and surrounding helium

bath. Thus,

$$\Sigma_{\pm} = (k - P)\sigma_0 \pm P\sigma_{\pm},$$

where  $\sigma_0$  represents the unpolarized proton cross section [ $\sigma_0 = \frac{1}{2}(\sigma_+ + \sigma_-)$ ] and  $k$  is the ratio of the average number of all nucleons (weighted by their unpolarized scattering power) to the number of free polarizable protons. Then the observed asymmetry  $A$  is related to the desired parameter  $\alpha$  by

$$A \equiv (\Sigma_+ - \Sigma_-) / (\Sigma_+ + \Sigma_-) = (P/k)\alpha.$$

The normalization is not a matter of critical importance, since the error involved is insignificant compared to the statistical uncertainty of the result. To get the asymmetry for a 100%-polarized free-proton target, corrections are made for (1) the scattering from target material other than free protons, evaluated by using known  $ep$  and  $en$  cross sections and the known target composition,  $k_1$ ; (2) scattering from material other than the target, evaluated by calculation in the same way,  $k_2$ ; (3) lack of exact orthogonality of the polarization vector and the scattering plane, evaluated by calculation,  $k_3$ ; and (4) radiative corrections which cause elastic scattering events to fall into the pion production region, evaluated by calculation using known data,<sup>18,19</sup>  $k_4$ .

The net normalization factor  $k$  is just the product of the four factors  $k_i$  (see Table II). It is useful to view the normalization in terms of a net target-polarization dilution factor. Thus, a 20% free-proton polarization corresponds to a net  $(20/k)\%$  target polarization. In this vein, the typical target polarization was about 2%. Thus, all raw counting asymmetries  $A$  must be multiplied by a factor on the order of 50 in order to get the physically meaningful asymmetry  $\alpha$ .

<sup>18</sup> C. Mistretta, D. Imrie, J. A. Appel, R. Budnitz, L. Carroll, M. Goitein, K. Hanson, and R. Wilson, Phys. Rev. Letters **20**, 1523 (1968); C. Mistretta, J. A. Appel, R. J. Budnitz, L. Carroll, J. Chen, J. R. Dunning, Jr., M. Goitein, K. Hanson, D. C. Imrie, and R. Wilson, Phys. Rev. **184**, 1487 (1969).

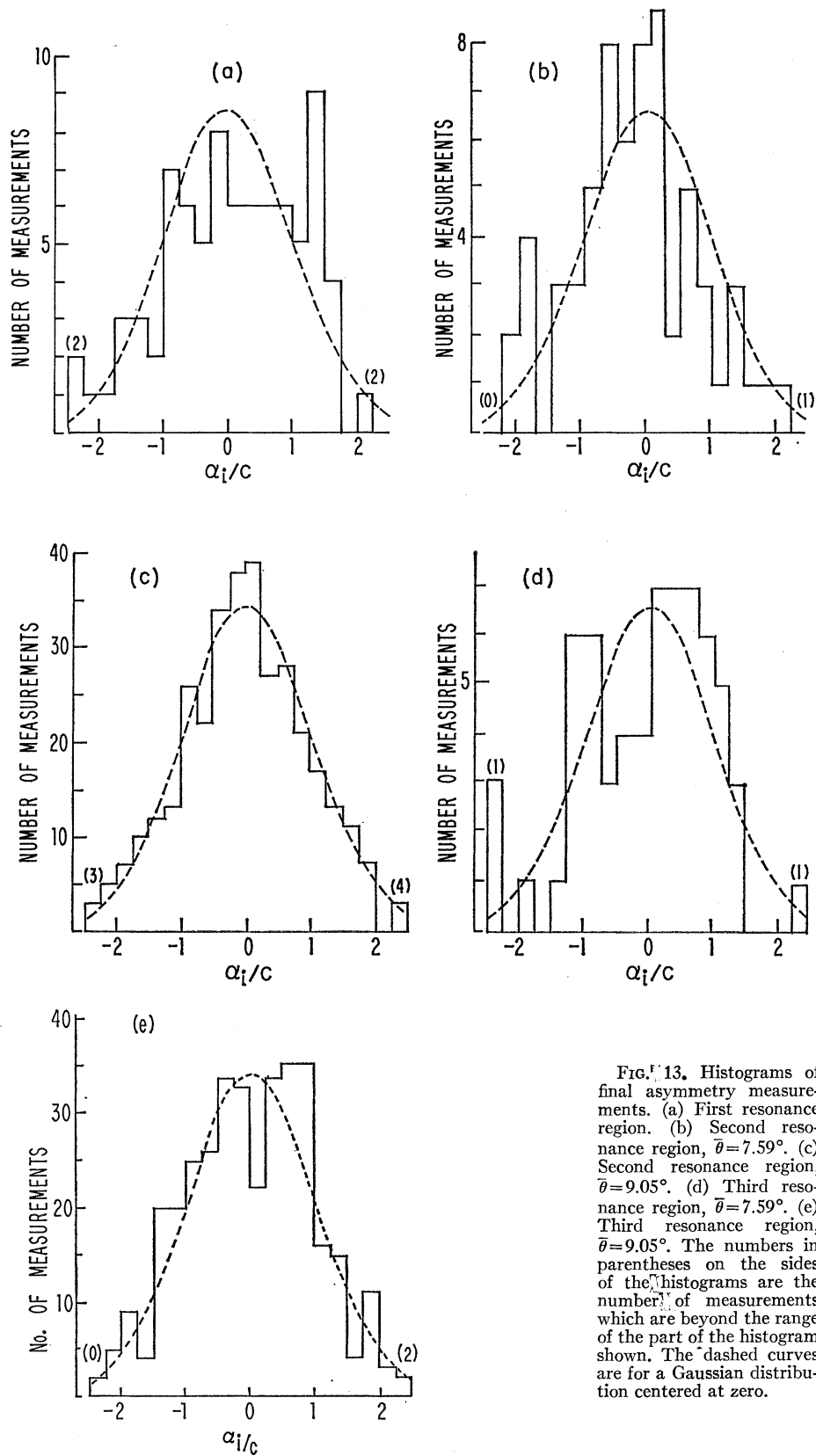


FIG. 13. Histograms of final asymmetry measurements. (a) First resonance region. (b) Second resonance region,  $\bar{\theta} = 7.59^\circ$ . (c) Second resonance region,  $\bar{\theta} = 9.05^\circ$ . (d) Third resonance region,  $\bar{\theta} = 7.59^\circ$ . (e) Third resonance region,  $\bar{\theta} = 9.05^\circ$ . The numbers in parentheses on the sides of the histograms are the number of measurements which are beyond the range of the part of the histogram shown. The dashed curves are for a Gaussian distribution centered at zero.

### III. RESULTS AND DISCUSSION

In this section the results of the asymmetry measurements are presented; the reliability of the data is checked and the results are interpreted in terms of the two possible  $T$ -violation models discussed in Sec. I.

The results are found to be insensitive to the particular biases selected in analyzing the data and there are no statistically significant variations of the asymmetry as a function of scattered-electron energy (or hadron final-state energy) in any of the resonance regions. The final results are shown to behave as expected for data whose principal uncertainty is statistical.

As a check, runs were grouped in such a way as to cancel any time-reversal-violating effects should they be present. This grouping, analyzed for an "asymmetry," gave results no different in character from the grouping used to reveal any time-reversal-violating effect.

Then a limit is placed on the relative phases of the scalar and transverse amplitudes for each of the two models discussed in Sec. I.

The asymmetries reported (Table III) have been calculated, in turn, from the numbers of computer triggers without reference to the computer analyses and from the final accepted event rates, corrected for the run-to-run variations in electron scattering angle, incident electron energy, and detailed computer analysis. The usual  $\chi^2$  per degree of freedom for the ensembles of asymmetry measurements appears in the tables under the heading  $\chi^2$ . The values of  $\chi^2$  per degree of freedom were also calculated assuming that the ensembles centered on zero, i.e., no evident violation. These values are listed under the heading  $\chi_0^2$ .

#### A. Asymmetry Results Sensitive to $T$ Violations

##### 1. Final Values and Effect of Various Corrections

The final values of the asymmetry are listed in Table III along with the asymmetries calculated from

TABLE II. Normalization factors.

| Electron scattering angle $\theta$ (deg) | Resonance region | $k_1$ | $k_2$ | $k_3$ | $k_4$ | $k$  |
|--|------------------|-------|-------|-------|-------|------|
| 7.34                                     | First            | 7.00  | 1.13  | 1.05  | 1.08  | 8.97 |
| 7.59                                     | Second and third | 7.00  | 1.13  | 1.05  | 1.04  | 8.64 |
| 9.05                                     | Second and third | 7.00  | 1.13  | 1.03  | 1.04  | 8.47 |

the computer trigger rates. The fluctuations of the incident energy and electron scattering angle are nearly negligible. The effect of the angular and energy corrections for run-to-run variations not only tend to cancel due to their randomness, but also are very small compared to the dominant statistical uncertainty of each run.

The application of computer analysis, however, is quite significant. Even though the computer triggering system had fairly rigid requirements, sufficient latitude remained that a significant fraction were not due to good scattering events. Their time distribution may well fluctuate widely, so it is no surprise that a significant improvement in  $\chi^2$  per degree of freedom was obtained by post-run computer analysis of the recorded data.

Histograms of the final asymmetry measurements are shown in Fig. 13.

##### 2. Various Computer-Analysis Requirements

The most significant part of the computer analysis is the requirement of an identifiable single-particle trajectory in the momentum-defining counters (Table IV). The standard set of biases used for the Čerenkov and shower counters contained little additional pulse-height requirements above those of the initial triggering circuitry (Figs. 7 and 8). However, an immediate improvement in  $\chi^2$  per degree of freedom occurs when

TABLE III. Final values and effect of run-to-run corrections.

| Resonance region | $\bar{\theta}$ (deg) | Number of asymmetry measurements | Type of rate used for $\alpha$ | Asymmetry $\alpha$ | Uncertainty $\delta\alpha$ | $\chi_0^2$ | $\chi_\alpha^2$ |
|------------------|----------------------|----------------------------------|--------------------------------|--------------------|----------------------------|------------|-----------------|
| First            | 7.34                 | 85                               | Computer trigger rate          | 0.079              | 0.024                      | 2.77       | 2.64            |
|                  |                      |                                  | Final values                   | 0.035              | 0.041                      | 1.50       | 1.49            |
| Second           | 7.59                 | 66                               | Computer trigger rate          | -0.091             | 0.045                      | 3.01       | 2.95            |
|                  |                      |                                  | Final values                   | -0.129             | 0.113                      | 1.13       | 1.11            |
|                  | 9.05                 | 343                              | Computer trigger rate          | 0.007              | 0.027                      | 1.40       | 1.40            |
|                  |                      |                                  | Final values                   | -0.005             | 0.057                      | 1.10       | 1.10            |
| Third            | 7.59                 | 66                               | Computer trigger rate          | -0.091             | 0.045                      | 3.01       | 2.95            |
|                  |                      |                                  | Final values                   | -0.005             | 0.099                      | 1.19       | 1.19            |
|                  | 9.05                 | 343                              | Computer trigger rate          | 0.007              | 0.027                      | 1.40       | 1.40            |
|                  |                      |                                  | Final values                   | -0.021             | 0.049                      | 1.04       | 1.04            |

TABLE IV. Effect of computer biases on asymmetry

| Resonance region | $\bar{\theta}$ (deg) | Čerenkov- and shower-counter levels | Momentum-def. codes accepted | Asymmetry $\alpha$ | Statistical uncertainty $\delta\alpha$ | $\chi_0^2$ | $\chi_\alpha^2$ | Number of asymmetry measurements |
|------------------|----------------------|-------------------------------------|------------------------------|--------------------|--|------------|-----------------|----------------------------------|
| First            | 7.34                 | Potential                           | trigger rate                 | 0.080              | 0.024                                  | 2.20       | 2.57            | 85                               |
|                  |                      | Standard                            | 00-11                        | 0.035              | 0.041                                  | 1.50       | 1.49            | 85                               |
|                  |                      | Standard                            | 00-10                        | 0.028              | 0.043                                  | 1.55       | 1.55            | 85                               |
|                  |                      | High                                | 00-11                        | 0.083              | 0.067                                  | 2.13       | 2.11            | 73                               |
| Second           | 7.59                 | Potential                           | trigger rate                 | -0.090             | 0.045                                  | 3.07       | 3.01            | 66                               |
|                  |                      | Standard                            | 00-11                        | -0.129             | 0.113                                  | 1.13       | 1.11            | 66                               |
|                  |                      | Standard                            | 00-11                        | -0.151             | 0.116                                  | 1.12       | 1.10            | 66                               |
|                  |                      | High                                | 00-11                        | -0.049             | 0.132                                  | 1.39       | 1.39            | 61                               |
|                  | 9.05                 | Potential                           | trigger rate                 | 0.007              | 0.027                                  | 1.36       | 1.35            | 343                              |
|                  |                      | Standard                            | 00-11                        | -0.005             | 0.055                                  | 1.10       | 1.10            | 343                              |
|                  |                      | Standard                            | 00-11                        | -0.035             | 0.060                                  | 1.12       | 1.12            | 340                              |
|                  |                      | High                                | 00-11                        | -0.071             | 0.075                                  | 1.08       | 1.07            | 285                              |
| Third            | 7.59                 | Potential                           | trigger rate                 | -0.090             | 0.045                                  | 3.07       | 3.01            | 66                               |
|                  |                      | Standard                            | 00-11                        | -0.005             | 0.099                                  | 1.19       | 1.19            | 66                               |
|                  |                      | Standard                            | 00-10                        | -0.011             | 0.102                                  | 1.20       | 1.20            | 66                               |
|                  |                      | High                                | 00-11                        | 0.049              | 0.118                                  | 1.43       | 1.43            | 61                               |
|                  | 9.05                 | Potential                           | trigger rate                 | 0.007              | 0.027                                  | 1.36       | 1.35            | 343                              |
|                  |                      | Standard                            | 00-11                        | -0.021             | 0.049                                  | 1.04       | 1.04            | 343                              |
|                  |                      | Standard                            | 00-10                        | -0.021             | 0.051                                  | 1.00       | 0.99            | 340                              |
|                  |                      | High                                | 00-11                        | -0.037             | 0.066                                  | 1.14       | 1.14            | 285                              |

momentum definition is required. This improvement is insensitive to the particular degree of imperfection accepted in the momentum-counter pattern. Requiring a clean momentum definition reduces the effects of general spray and random end-bin triggers. Adding higher Čerenkov- and shower-counter pulse-height biases has little effect on the asymmetry. The singles

rates in the momentum-definition counters were significantly higher in this experiment than in any previous experiment with the same detection apparatus. The singles rates in the trigger counters were on the order of 1 Mc/sec. To reduce the random-coincidence trigger effects, only data for events with four or more momentum-defining counters expected to fire were used in the computer-analyzed data.

The cause of the high singles rates in the counters was the spray of low-energy particles resulting from the large magnetic field at the target. Nevertheless, the combination of momentum definition, Čerenkov- and shower-counter requirements was sufficient to provide an unbiased sample of scattered-electron events. The detection system was operated at intensities where it behaved in a generally unambiguous and stable mode (Figs. 5 and 6).

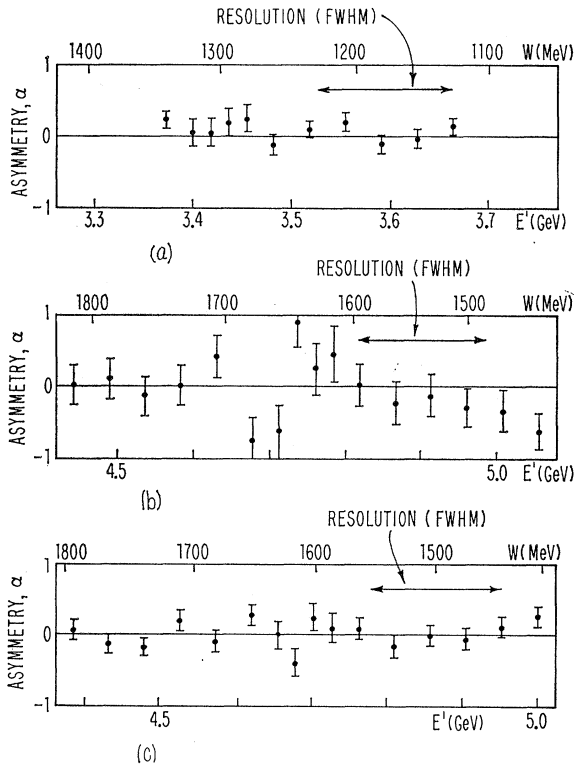


FIG. 14. Asymmetry spectra. (a)  $\bar{\theta}=7.34^\circ$ . (b)  $\bar{\theta}=7.59^\circ$ . (c)  $\bar{\theta}=9.05^\circ$ .

TABLE V. Trajectory separation.

| Resonance region | $\bar{\theta}$ (deg) | Trajectory type <sup>a</sup> | Asymmetry $\alpha$ | Statistical uncertainty $\delta\alpha$ | $\chi_0^2$ | $\chi_\alpha^2$ |
|------------------|----------------------|------------------------------|--------------------|--|------------|-----------------|
| First            | 7.34                 | <i>a+b</i>                   | 0.035              | 0.043                                  | 1.50       | 1.49            |
|                  |                      | <i>a</i>                     | -0.031             | 0.068                                  | 0.96       | 0.95            |
|                  |                      | <i>b</i>                     | 0.093              | 0.065                                  | 1.35       | 1.33            |
| Second           | 7.59                 | <i>a+b</i>                   | -0.129             | 0.113                                  | 1.13       | 1.11            |
|                  |                      | <i>a</i>                     | -0.253             | 0.165                                  | 1.16       | 1.13            |
|                  |                      | <i>b</i>                     | -0.006             | 0.161                                  | 1.03       | 1.03            |
|                  | 9.05                 | <i>a+b</i>                   | -0.005             | 0.057                                  | 1.10       | 1.10            |
|                  |                      | <i>a</i>                     | 0.042              | 0.085                                  | 1.02       | 1.01            |
|                  |                      | <i>b</i>                     | -0.046             | 0.082                                  | 1.04       | 1.04            |
| Third            | 7.59                 | <i>a+b</i>                   | -0.005             | 0.099                                  | 1.19       | 1.19            |
|                  |                      | <i>a</i>                     | -0.019             | 0.145                                  | 0.84       | 0.84            |
|                  |                      | <i>b</i>                     | 0.006              | 0.142                                  | 1.14       | 1.14            |
|                  | 9.05                 | <i>a+b</i>                   | -0.021             | 0.049                                  | 1.04       | 1.04            |
|                  |                      | <i>a</i>                     | -0.165             | 0.072                                  | 1.00       | 0.98            |
|                  |                      | <i>b</i>                     | 0.120              | 0.071                                  | 1.01       | 1.01            |

<sup>a</sup> *a* = above; *b* = below.

TABLE VI. Systematic checks.

| Resonance region | $\bar{\theta}$ (deg) | Number of asymmetry measurements | Type of asymmetry | Asymmetry $\alpha$ | Statistical uncertainty $\delta\alpha$ | $\chi_0^2$ | $\chi_\alpha^2$ |
|------------------|----------------------|----------------------------------|-------------------|--------------------|--|------------|-----------------|
| First            | 7.34                 | 85                               | Regular           | 0.035              | 0.043                                  | 1.50       | 1.49            |
|                  |                      | 85                               | Chron.            | -0.009             | 0.043                                  | 1.50       | 1.50            |
|                  |                      | 37                               | Double-posn. arg. | -0.012             | 0.044                                  | 1.78       | 1.78            |
| Second           | 7.59                 | 66                               | Regular           | -0.129             | 0.113                                  | 1.13       | 1.11            |
|                  |                      | 66                               | Chron.            | 0.073              | 0.113                                  | 1.13       | 1.12            |
|                  |                      | 20                               | Double-posn. arg. | -0.075             | 0.145                                  | 1.56       | 1.54            |
|                  | 9.05                 | 343                              | Regular           | -0.005             | 0.057                                  | 1.10       | 1.10            |
|                  |                      | 343                              | Chron.            | -0.032             | 0.057                                  | 1.10       | 1.10            |
|                  |                      | 153                              | Double-posn. arg. | -0.117             | 0.062                                  | 1.06       | 1.04            |
| Third            | 7.59                 | 66                               | Regular           | -0.006             | 0.099                                  | 1.19       | 1.19            |
|                  |                      | 66                               | Chron.            | -0.058             | 0.099                                  | 1.19       | 1.19            |
|                  |                      | 20                               | Double-posn. arg. | 0.090              | 0.126                                  | 1.09       | 1.09            |
|                  | 9.05                 | 343                              | Regular           | -0.021             | 0.049                                  | 1.04       | 1.04            |
|                  |                      | 343                              | Chron.            | -0.012             | 0.049                                  | 1.04       | 1.04            |
|                  |                      | 153                              | Double-posn. arg. | -0.006             | 0.053                                  | 1.07       | 1.07            |

### 3. Asymmetry Spectra

The asymmetry as a function of scattered-electron energy  $E'$  and hadron center-of-mass energy  $W$  is given in Fig. 14. In interpreting these spectra it should be remembered that the scattered-electron energy resolution (FWHM) was about 4%. Thus, we could not resolve structure as fine as the abrupt irregularities in the middle of the spectrum at  $\theta=7.59^\circ$ . Furthermore, because of the momentum-definition system, adjacent energy bins are highly anticorrelated.

This presentation is another way of expressing the asymmetry presented in the previous section as an average over the region of each resonance. We might note that none of the models which inspired this experiment has rapid variation of the asymmetry as a function of hadron energy.

### 4. Trajectory Separation

The results of the separate analyses of the events with electrons scattered above and below the horizontal plane are shown in Table V.

Since the upper and lower apertures are symmetric with respect to the scattering plane, the summed counting rate is potentially less sensitive to instabilities than either of the separate trajectory rates. However, the values of  $\chi^2$  per degree of freedom show only small and

inconsistent differences for the separate and summed trajectory data. Furthermore, no systematic differences in the handling of the two types of events have been discovered.

The separate trajectory asymmetries taken alone do not show significant  $T$ -violation effects.

### B. Systematic Checks Insensitive to $T$ Violations

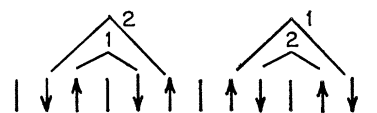
In order to check possible systematic biases and to see what general behavior may be ascribed to the electron beam and detection system, analyses have been made of two groupings of the runs which would cancel any  $T$ -violation effect. These specially constructed asymmetries are made insensitive to the



(a)



(b)



(c)

TABLE VII. Reversed-field runs.

| $\bar{\theta}$ (deg) | (Reversed-field rate)/(scattered electron rate) |   |
|----------------------|---|---|
|                      | Ratio of computer trigger rates (%)             | Ratio of final accepted event rates (%) |
| 7.59                 | 7.0   | 0.4                                     |
| 9.05                 | 1.2   | 0.4                                     |

FIG. 15. Experimental-run ordering. (a) Standard order. (b) Early-run order. (c) Double-position-averaged order.

TABLE VIII. First-resonance-region  $R$  values.

| Four-momentum transfer $q^2$ (GeV/c) <sup>2</sup> | $\sigma_T(q^2)$ (b) | $\sigma_0(q^2)$ (b) | Ref.    | $R = (\sigma_0/\sigma_T)^{1/2}$        |
|---|---------------------|---------------------|---------|--|
| 0.1   | 530±52              | 62 ±27              | 18      | 0.34 <sub>-0.18</sub> <sup>+0.08</sup> |
| 0.2   | 444±13              | 88 ±23              | 18      |  |
|   | 436±23              | 115 ±37             | 19      |  |
|   | 442±11              | 95 ±20              | Average | 0.46 <sub>-0.06</sub> <sup>+0.05</sup> |
| 0.3   | 393±14              | 144 ±31             | 18      |  |
|   | 402±18              | 81 ±34              | 19      |  |
|   | 396±11              | 115.4±23            | Average | 0.54 <sub>-0.06</sub> <sup>+0.05</sup> |

$T$ -violation effect by averaging out effects which are correlated with the sign of the target polarization.

### 1. Chronologically Ordered Asymmetry

The chronologically ordered asymmetry was obtained by taking the first minus the second cross-section measurement of each pair at a given target position. This difference divided by the sum of cross sections gives an asymmetry in which, for the pattern given in Sec. II, spin-correlated effects will average to zero. However, this asymmetry will be sensitive to linear drifts in the system.

### 2. Double-Target-Position-Averaged Asymmetry

The double-target-position-averaged asymmetry was obtained by summing events from paired adjacent runs before calculating an asymmetry. The summation is indicated schematically by the brackets in Fig. 15(c).

The sum of cross sections from the paired runs in Fig. 15(c) was calculated as indicated by

$$\alpha = (1-2)/(1+2).$$

The first sum minus the second, divided by the sum of all four cross sections, gives an asymmetry which is independent of polarization-correlated effects and, for the sequence in Fig. 15, linear-drift effects, too. This analysis is somewhat more sensitive than the actual bias analysis to target-thickness effects. However, since adjacent target positions have about  $\frac{2}{3}$  of the beam going through identical locations for both positions, this is not expected to introduce any substantial systematic asymmetry.

### 3. Conclusions

The specially constructed asymmetries of this section (Table VI) are most useful as indicators of the performance of the experimental apparatus independent of any polarization effects. Thus, the most significant conclusion of this section is that the statistical behavior of the results is independent of the polarization. For example, the somewhat improbable  $\chi^2$  per degree of freedom for the results in the first resonance region carry over from the  $T$ -violation asymmetry to the

special asymmetries of this section. Thus, the  $T$ -violation-sensitive results are essentially indistinguishable from the other asymmetries.

### C. Possible Pion Contamination

Pion contaminations of the scattered electrons and electrons from Dalitz decay of neutral pairs are possible asymmetry-producing backgrounds in this experiment. A polarization asymmetry is in general expected for detection of a restricted hadron phase space associated with a given scattered-electron energy. Pion contamination in this experiment would be the result of such a restricted pion acceptance, but would be integrated over all (undetected) scattered-electron energies.

As a check of neutral-pion-initiated events (and general spray), short runs were taken with the polarity of the half-quadrupole magnet reversed. The results are shown in Table VII. Assuming that an equal number of apparent positron and electron events result from neutral-pion decay, these events accounted for less than 0.5% of the accepted electron events. Even for a maximum polarization correlation for this contamination, the effect on the final result would be less than  $\frac{1}{10}$  of a standard deviation.

The lack of significant change in the resultant asymmetry when the Čerenkov- and shower-counter bias requirements were significantly raised is evidence that the results are unaffected by possible charged-pion contamination.

The above two evidences are taken as sufficient indication that the results of this experiment are not affected by any possible pion contamination remaining in the accepted sample. No subtractions or increases in uncertainty were made due to possible pion contamination.

### D. Interpretation of Results

#### 1. First Resonance Region

*a. Maximal effect.* Assuming that both resonant and nonresonant amplitudes contribute to a time-reversal-violation asymmetry, an estimate of the maximal effect possible for this experiment can be obtained. Estimates of  $A$  and  $R$  [Eq. (12)] are needed to determine the phase angle between the potentially interfering scalar and transverse amplitudes in this model. Lynch *et al.*<sup>10</sup> and Pevez-y-Jorba *et al.*<sup>11</sup> have separated the scalar and transverse contributions to the cross section in the kinematic range of interest. From their values (Table VIII),  $R = (\sigma_0/\sigma_T)^{1/2} \sim 0.5$  near  $q^2 = 0.23$  (GeV/c)<sup>2</sup>.

Since the transverse pion production amplitudes in this region are dominated by the resonance, the value of  $A$  can be approximated by the resonant amplitude only. For the resonant magnetic dipole excitation,<sup>5,20</sup>

<sup>20</sup> K. Baba, N. Kajiura, S. Kaneko, K. Huke, R. Kikuchi, Y. Kobayashi, and T. Yamakamo, INS Japan Report, 1968 (unpublished).

$F_+ = \sqrt{3}F_-$  and  $A = \frac{1}{2}$ . From Eq. (13),

$$\sin\delta = \alpha(1+R^2)/2AR = 2.5\alpha,$$

which leads to  $\delta = (4.9_{-5.9}^{+6.2})^\circ$ .

*b. Pure resonant effect.* If one assumes that a  $T$ -violation effect occurs in the resonance alone, i.e., only the resonant part of  $F_-$  interferes with only the resonant part of  $F_+$ , one gets a slightly less restrictive limit on  $\sin\delta$ . A maximal effect within the confines of the purely resonant model occurs if all the scalar amplitude is resonant (in agreement with the tentative results of Mistretta *et al.*<sup>12</sup> for the  $\pi^0$ , but not including all parts of the pion pole contribution for  $\pi^+$  production). Further, we extend the result of photoproduction by taking 75% of the transverse production as resonant; then  $f_1 = \sqrt{(0.75)}$  and  $f_2 = 1.0$ , so that  $\sin\delta = \alpha(1+R^2)/2f_1f_2AR = 2.9\alpha$  and  $\delta = (5.8_{-6.9}^{+7.2})^\circ$ .

### 2. Second Resonance Region

*a. Maximal effect.* From a recent compilation of photoproduction data,<sup>13</sup> the total  $\gamma p$  cross section is about 125  $\mu\text{b}$  in the region of the second resonance. Taking this value for  $\sigma_T(q^2=0)$  and applying a  $q^2$  dependence of the form

$$G_{Mp}(q^2)/G_{Mp}(0) = 1/(1+q^2/0.71)^2$$

gives values for the transverse cross section  $\sigma_T(q^2)$  in the regions of interest here. Taking the value of the total cross section from Cone *et al.*<sup>13</sup> at  $q^2 = 0.79$  (GeV/c)<sup>2</sup> and  $\epsilon = 0.72$  as appropriate to both the experimental points gives the value of the total scalar cross section  $\sigma_0$  from (shown in Table IX)  $\sigma = \sigma_T + \epsilon\sigma_0$ . Some recent measurements<sup>21</sup> confirm that neither  $\sigma_0$  nor  $\sigma_T$  is zero in this region.  $\sigma_0/\sigma_T$  lies between  $\frac{1}{4}$  and 4.

The resonance does not contribute to the numerator of  $A$  since  $(F_-)_{\text{res}} = 0$ . The deduction that  $F_- = 0$  comes from the nonobservation of the resonance in 180° photoproduction.<sup>22</sup> Thus, even a maximal effect includes only interference of the resonant and nonresonant scalar amplitudes with part of the nonresonant transverse amplitudes. Thus, in order to obtain an estimate of the maximal asymmetry consistent with current knowledge, we assume that (1)  $(F_+)_{\text{nonres}} = 0$  and (2) all scalar amplitudes participate in the interference. Thus,  $f_2 = 1$ , and from the data of Cone *et al.*,  $Af_1 = 0.6$ . Thus, for  $q^2 = 0.52$  (GeV/c)<sup>2</sup>,

$$\sin\delta = (1.9)\alpha \quad \text{and} \quad \delta = (-15_{-13}^{+14})^\circ$$

and, for  $q^2 = 0.72$  (GeV/c)<sup>2</sup>,

$$\sin\delta = (2.1)\alpha \quad \text{and} \quad \delta = (-0.5 \pm 6.9)^\circ.$$

*b. Pure resonant effect.* For  $(F_-)_{\text{res}} = 0$  as discussed above, there can be no purely resonant  $T$ -violation effect evident in this experiment.

<sup>21</sup> M. Goitein *et al.* (private communication). This is in agreement with the expected electric dipole excitation of the resonance.

<sup>22</sup> J. T. Beale, S. D. Ecklund, and R. L. Walker, Cal. Tech. Report No. CTSL-42 (CALT-68-108) (unpublished).

TABLE IX. Second-resonance-region ratio of scalar to transverse amplitudes.

| Four-momentum transfer $q^2$ (GeV/c) <sup>2</sup> | $\sigma_T(q^2)$ ( $\mu\text{b}$ ) | $\sigma$ ( $\mu\text{b}$ ) | $\sigma_0$ ( $\mu\text{b}$ ) | $R = (\sigma_0/\sigma_T)^{1/2}$ |
|---|-----------------------------------|----------------------------|------------------------------|---------------------------------|
| 0.52  | 42                                | 120                        | 108                          | 1.6                             |
| 0.72  | 31                                | 120                        | 123                          | 2                               |

### 3. Third Resonance Region

Data on the third resonance region are even more sparse than for the second resonance region. Thus, to make an estimate of  $\sin\delta$  from the value of  $\alpha$ , it is necessary to make even more extrapolations. We again theoretically expect both longitudinal and transverse scattering to contribute. From the indications that  $(F_-)_{1688 \text{ res}} = 0$ ,<sup>22</sup> we again find the purely resonant effect vanishes. The maximum-effect model discussed is similar to that discussed for the second resonance region. Thus  $f_2 = 1$ , and, from the data of Cone *et al.*,<sup>13</sup>  $Af_1 = 0.5$ . Furthermore, the value of  $(1+R^2)/R$  which occurred for both other resonance regions is used. Thus, at  $q^2 = 0.49$  (GeV/c)<sup>2</sup>,  $\sin\delta = (2.5)\alpha$ ; whence  $\delta = (-1_{-15}^{+13})^\circ$ , and, at  $q^2 = 0.68$ ,  $\delta = (-3.0 \pm 7.1)^\circ$ .

The amplitudes  $F^+$  and  $F^-$  are real over the whole resonance region in absence of  $T$  violation. It seems plausible to consider a  $T$ -violating phase which changes sign from one side of the resonance to the other, passing through zero on the resonance. Figure 14 shows no such effect.

### E. Conclusions of Experiment

The results of this experiment are summarized in Table X. Values of  $\delta$  away from zero imply violation of  $T$  invariance.

From these results, it is clear that any  $T$  violation is less than maximal for the regions studied in this experiment, by a factor of about 10. Furthermore, there is no evidence of any  $T$  violation outside the precision of this experiment.

We note that at the first resonance,  $\Delta I = 1$  electromagnetic current is predominant, whereas for the other two  $\Delta I = 0$  is involved.

In order to explain the magnitude of the observed  $CP$  violation in the decay of the long-lived neutral  $K$  meson via the electromagnetic Hamiltonian, a nearly maximal  $T$  violation in the electromagnetic Hamiltonian was assumed. We find no such maximal violation evident and, therefore, no evidence for the hypothesized  $T$ -even current  $K$  suggested by Bernstein, Feinberg, and Lee.<sup>2</sup>

### F. Other Direct Tests of $T$ Invariance of $H_\gamma$

Four other types of experiment have been performed relating directly to the  $T$  invariance of the electromagnetic interactions: (1) measurements of the angular

TABLE X. Summary.

| Resonance region | $\bar{\theta}$ (deg) | Asymmetry $\alpha$ | Model     | Fraction of maximal violation | Phase angle $\delta$ (deg) |
|------------------|----------------------|--------------------|-----------|-------------------------------|----------------------------|
| First            | 7.34                 | $0.035 \pm 0.043$  | Max. eff. | $0.088 \pm 0.105$             | $4.9_{-5.9}^{+6.2}$        |
|                  |                      |                    | Pure res. | $0.102 \pm 0.119$             | $5.8_{-6.9}^{+7.2}$        |
| Second           | 7.59                 | $-0.129 \pm 0.113$ | Max. eff. | $-0.245 \pm 0.215$            | $-15.0_{-13}^{+14}$        |
|                  |                      |                    | Max. eff. | $-0.009 \pm 0.120$            | $0.5_{-6.9}^{+6.9}$        |
| Third            | 7.59                 | $-0.005 \pm 0.099$ | Max. eff. | $-0.014 \pm 0.247$            | $-1.0_{-15}^{+13}$         |
|                  |                      |                    | Max. eff. | $-0.052 \pm 0.123$            | $-3.0 \pm 7.1$             |

and polarization dependence of  $\gamma$ -ray absorption and emission using Mössbauer nuclei,<sup>23,24</sup> (2) searches for the electric-dipole-moment interaction of the neutron,<sup>25,26</sup> (3) measurement of the recoil-deuteron vector polarization in elastic electron-deuteron scattering,<sup>27</sup> and (4) reciprocity test in the angular distributions of the reactions  $\gamma + d \rightleftharpoons n + p$ .<sup>28</sup> Results from the first three experiments have been published and reveal no violations of time-reversal invariance. No conclusive evidence is yet available from the preliminary analyses of the fourth type of experiment.

So-called maximal effects have been predicted for each of the above tests. In each case, a phenomenological model is used which contains an arbitrary parameter. Allowing the arbitrary parameter to take the largest value consistent with physical laws and present measurements leads to a "predicted maximal effect." The maximal effects for each experiment have typically been made in advance of experimental results and are usually rather less than conservative. Nevertheless, such maximal estimates do give some gauge of the relative sensitivity of the various experiments (see Table XI). On this basis, the limit on time-reversal violations from the neutron electric-dipole-moment experiment is clearly the most useful. However, both the neutron electric-dipole-moment experiment and the experiments on the nuclear matrix elements are essentially low-energy tests and there is no *a priori* reason why any time-reversal violation should be independent of energy. One must have a very specific model for any violation before extrapolating from one energy region or, indeed, from one type of experiment to another. Such detailed models await positive evidence of a violation.

Thus, the high-energy tests must be viewed separately from those at lower energy. The experiment reported here is a direct test of  $T$  invariance in the  $\gamma NN^*$  vertex. Barshay<sup>28</sup> invokes a maximal violation of time-reversal invariance in just this vertex in calculating

<sup>23</sup> O. C. Kistner, Phys. Rev. Letters **19**, 872 (1967).

<sup>24</sup> M. Alta, B. Chrisman, P. de Brunner, and H. Frauenfelder, Phys. Rev. Letters **20**, 691 (1968).

<sup>25</sup> J. K. Baird, P. D. Miller, W. B. Dress, and N. F. Ramsey, Phys. Rev. **179**, 1285 (1969).

<sup>26</sup> C. G. Shull and R. Nathans, Phys. Rev. Letters **19**, 384 (1967).

<sup>27</sup> R. Prepost, R. M. Simonds, and B. H. Wiik, Phys. Rev. Letters **21**, 1271 (1968).

<sup>28</sup> S. Barshay, Phys. Rev. Letters **17**, 49 (1966).

TABLE XI. Other experimental tests of  $H_\gamma$ .

| $T$ -test technique                   | Maximum effect        | Experimental result             | Ref. |
|---------------------------------------|-----------------------|---------------------------------|------|
| Mössbauer Ru <sup>99</sup> asymmetry  | $10^{-2}$ – $10^{-3}$ | $(-1.0 \pm 1.7) \times 10^{-3}$ | 23   |
| Mössbauer Ir <sup>193</sup> asymmetry |                       | $(1.1 \pm 3.8) \times 10^{-3}$  | 24   |
| Electric dipole moment                | $10^{-19}$ e cm       | $5 \times 10^{-22}$ e cm        | 25   |
| $e$ - $d$ scattering asymmetry        | 0.34                  | $0.075 \pm 0.088$               | 27   |

the size of any expected effect for the  $\gamma + d \rightleftharpoons n + p$  comparison. The electron-deuteron elastic scattering contains the same vertex, at least, in higher-order diagrams. There are, however, relevant differences. The photon in the  $\gamma + d \rightleftharpoons n + p$  comparison is real and an effect is obtained in interference between different angular momentum states of the final  $n$ - $p$  system. In this electron scattering experiment an effect requires that the relevant photon be virtual. Since one is looking for interference between transverse and scalar components of the fields, one specifically integrates over all final hadron states.

What can now be said is that the time reversal is not violated in a universally maximal fashion, even in the restricted area of the electromagnetic interactions of the hadrons. More subtle models of  $T$  violation will undoubtedly await more exact experimental evidence.

#### ACKNOWLEDGMENTS

The authors wish to thank the Harvard cyclotron staff and shops and the Cambridge Electron Accelerator staff for their valuable assistance throughout all phases of this experiment.

#### APPENDIX

During the course of preparations for the time-reversal experiment, consideration was given to detecting the recoiling charged hadrons. These considerations were directed at obtaining information on single-pion production in the region of the first resonance via measurement of the asymmetry of cross sections differential in hadron and electron parameters (decay asymmetry). Such an asymmetry is expected even with time-reversal invariance.

Interest in determining such asymmetries lies in (1) the possibility of extracting the charged-pion form factor and (2) more sensitive measurements of the non-resonant amplitudes than available through previous experiments.<sup>19</sup> Since the decay asymmetry is proportional to the imaginary part of the interference between relevant amplitudes, it is particularly sensitive to interferences between the well-known resonant amplitudes and the less-well-known nonresonant amplitudes. Extraction of information from this type of interference would serve as a useful independent check on the

theories used to extract the pion form factor and various partial-wave amplitudes from single-pion electroproduction.<sup>19</sup>

The interest in coincident measurement of recoiling hadrons was given up when it became clear that the high magnetic field of the polarized target was sweeping forward-produced low-energy particles into the

solid angle of interest for coincident hadrons. A separate sweeping magnet was needed to protect the intended hadron counters but was unavailable. In future experiments, it is possible that a magnetic field used to shield the hadron counters will also serve usefully to momentum-analyze the recoiling particles and thereby provide particle identification.

PHYSICAL REVIEW D

VOLUME 1, NUMBER 5

1 MARCH 1970

### $\pi^+\pi^-\pi^0$ Decay of 1138 $\eta$ Mesons Produced in $K^-, p \rightarrow \Lambda, \eta$ near Threshold\*

D. W. CARPENTER, M. E. BINKLEY, J. W. CHAPMAN,† B. B. COX,‡ S. DAGAN,§ L. R. FORTNEY, E. C. FOWLER, J. P. GOLSON, J. E. KRONENFELD, Z. -M. MA,|| C. M. ROSE, W. M. SMITH, AND T. R. SNOW  
*Department of Physics, Duke University, Durham, North Carolina 27706*

(Received 17 November 1969)

The Dalitz plot density of  $\eta \rightarrow \pi^+\pi^-\pi^0$  is examined. We find the asymmetry on the  $\pi^\pm$  energies to be  $A = (N^+ - N^-)/(N^+ + N^-) = -0.014 \pm 0.030$ , where  $N^\pm$  is the number of events for which  $T_\mp > T_\mp$ . The density is well fitted with a linear dependence on  $T_0$ :  $|M|^2 \propto 1 + 2\alpha[(3T_0/Q) - 1]$ , with  $\alpha = -0.47 \pm 0.04$ .

#### INTRODUCTION

HAVING captured the special interest of physicists as the first success of "the eightfold way,"<sup>1</sup> the  $\eta$  meson has retained this interest because it is the only hadron whose decay to hadronic final states is known to be mediated by the electromagnetic interactions.<sup>2</sup> The Duke group has completed a study of 1138 examples of the  $\pi^+\pi^-\pi^0$  decay of  $\eta$  mesons.<sup>3</sup> Because they were produced in a hydrogen bubble chamber via  $K^- + p \rightarrow \Lambda + \eta$  near threshold ( $\approx 740$  MeV/c), this sample of  $\eta$

meson decays is particularly free from background. Further, since scanners first searched for the readily recognizable  $\Lambda \rightarrow p + \pi^-$  decay, there is an almost constant efficiency of observation for the various configurations of  $\pi^+\pi^-\pi^0$  in the final sample. All of the information characterizing these decays is contained in the Dalitz-Fabri plot of Fig. 2. Results of two analyses are of particular interest.

(1) The asymmetry in the energy between  $\pi^+$  and  $\pi^-$  is  $A = (N^+ - N^-)/(N^+ + N^-) = -0.014 \pm 0.030$ , where  $N^\pm$  is the number of events in which the kinetic energy of the  $\pi^\pm$  is greater than that of the  $\pi^\mp$ . This result is compatible with either  $C$  conservation or  $C$  nonconservation to the extent observed by Lee and his collaborators.<sup>4</sup>

(2) The number of events per unit area on the Dalitz plot may be adequately described by a linear function of the neutral pion's kinetic energy,  $T_0$ . For the square of the matrix element  $|M|^2 \propto 1 + 2\alpha y$ , with  $y = (3T_0/Q) - 1$ , and  $Q = M(\eta) - M(\pi^+) - M(\pi^-) - M(\pi^0)$ , we find  $\alpha = -0.47 \pm 0.04$ . This is in agreement with previous

\*The research leading to this report was carried out at the Brookhaven National Laboratory and Duke University with partial financial support of the U. S. Atomic Energy Commission.

† Present address: University of Michigan, Ann Arbor, Mich.

‡ Present address: Johns Hopkins University, Baltimore, Md.

§ Present address: TECHNION (Israel Institute of Technology), Haifa, Israel.

|| Present address: Michigan State University, East Lansing, Mich.

<sup>1</sup> A. Pevsner, R. Kraemer, M. Nussbaum, C. Richardson, P. Schlein, R. Strand, T. Toohig, M. Block, A. Engler, R. Gessaroli, and C. Meltzer, Phys. Rev. Letters **7**, 421 (1961); M. Gell-Mann, California Institute of Technology Synchrotron Laboratory Report No. CTS-20, 1961 (unpublished); M. Gell-Mann, Phys. Rev. **125**, 1067 (1962); P. L. Bastien, J. P. Berge, O. I. Dahl, M. Ferro-Luzzi, D. H. Miller, J. J. Murray, A. H. Rosenfeld, and M. B. Watson, Phys. Rev. Letters **8**, 114 (1962).

<sup>2</sup> For reviews, see G. Salvini, Rivista Del Nuovo Cimento **1**, 57 (1969); C. Baltay, in *Meson Spectroscopy* (W. A. Benjamin, Inc., New York, 1968).

<sup>3</sup> Preliminary reports have been made by this group on partial samples: E. C. Fowler, Bull. Am. Phys. Soc. **11**, 380 (1966); L. R. Fortney, J. W. Chapman, S. Dagan, and E. C. Fowler, in *Proceedings of the Thirteenth Annual International Conference on High-Energy Physics, Berkeley, Calif., 1966* (University of California Press, Berkeley, Calif., 1967); B. B. Cox, L. R. Fortney, D. W. Carpenter, C. M. Rose, W. Smith, and E. C. Fowler, Acta Phys. Austriaca Suppl. V, 477 (1968).

<sup>4</sup> M. Gormley, E. Hyman, W. Lee, T. Nash, J. Peoples, C. Schulz, and S. Stein, Phys. Rev. Letters **21**, 402 (1968) ( $A = 0.015 \pm 0.005$ ); **22**, 108 (1969); A. M. Cnops, G. Finocchiaro, J. C. Lassalle, P. Mittner, P. Zanella, J. P. Dufey, B. Gobbi, M. A. Pouchon, and M. Müller, Phys. Letters **22**, 546 (1966) ( $A = 0.003 \pm 0.011$ ); C. Baltay, P. Franzini, J. Kim, L. Kirsch, D. Zanello, J. Lee-Franzini, R. Loveless, J. McFadyen, and H. Yarger, Phys. Rev. Letters **16**, 1224 (1966) ( $A = 0.072 \pm 0.028$ ); A. Larribe, A. Leveque, A. Muller, E. Pauli, D. Revel, T. Tallini, P. J. Litchfield, L. K. Rangan, A. M. Segar, J. R. Smith, P. J. Finney, C. M. Fisher, and E. Pickup, Phys. Letters **23**, 600 (1966) ( $A = -0.061 \pm 0.040$ ); Columbia-Berkeley-Purdue-Wisconsin-Yale Collaboration, Phys. Rev. **149**, 1044 (1966) ( $A = 0.058 \pm 0.034$ ).